Stochastic Transmission Expansion Planning Considering Uncertain Dynamic Thermal Rating of Overhead Lines

Junpeng Zhan, *Member, IEEE*, Weijia Liu, and C. Y. Chung, *Fellow, IEEE*

***Abstract*—Dynamic thermal rating (DTR) is an important smart grid technology that can bring considerable economic benefits. One of the most important benefits of DTR is to postpone new investment. This paper proposes a novel stochastic transmission expansion planning (STEP) model considering the DTR of overhead lines. The objective function of the STEP model includes operational costs and the investment costs of new line construction and DTR systems installation. The model can determine where to build new lines and install DTR systems. The model can not only realize the benefits that occur when the DTR is higher than the static thermal rating (STR) but also avoid overload risk, i.e., the power flow on a line being larger than the line's real capacity, caused by the DTR being lower than the STR. The model can consider both the voltage magnitude and phase angle of each bus. The model is linearized and therefore can be effectively solved by a Benders decomposition method. Furthermore, a new way of scenario reduction is proposed to obtain a better set of reduced scenarios. The effectiveness of the model is verified on a modified IEEE reliability test system and a modified IEEE 300-bus system.**

***Index Terms*—Dynamic thermal rating (DTR); overload risk; static thermal rating (STR); scenario reduction; stochastic programming; transmission expansion planning (TEP).**

NOMENCLATURE

Acronyms

DCPF	DC power flow
DLPF	Decoupled linearized power flow
DTR	Dynamic thermal rating
IFSA	Improved forward selection algorithm
LTE	Long-term emergency rating
NYPA	New York Power Authority
RS	Reduced scenario
RTS	Reliability test system
RoW	Right-of-way
STE	Short-term emergency rating
STR	Static thermal rating
STEP	Stochastic transmission expansion planning
TEP	Transmission expansion planning

Sets/Indices

$g \in \Omega_G$	Generators excluding wind generation
$\mathrm{i} \in \Omega_\mathrm{B}$	Buses
$(i,g) \in \boldsymbol{\Lambda}$	Incidence between bus i and generator g
$l \in \Omega, \Omega_1$	RoW: Ω denotes all RoWs and Ω_1 denotes the set of RoW where at least one line is in operation, regardless of whether initially or newly installed
$\kappa \in \Omega_{rs}$	The κth RS associated with uncertainties of wind, electricity load demand, and DTR
$\boldsymbol{X}^\kappa, \boldsymbol{Y}$	Spaces for 2nd- and 1st-stage decision variables
ξ	Iteration in Benders decomposition (integer)
Ω_{rs} (Ω_{os})	Reduced (original) set of scenarios
D (S)	Superscripts representing DTR (STR)

The work was supported in part by the Natural Sciences and Engineering Research Council (NSERC) of Canada and the Saskatchewan Power Corporation (SaskPower). All the authors are with the Department of Electrical and Computer Engineering, University of Saskatchewan, Saskatoon, SK S7N 5A9, Canada (e-mail: zhanjunpeng@gmail.com, liuweijiamarcel@gmail.com, c.y.chung@usask.ca).

Variables

f_l^κ	Active power flow at a line in RoW l (MW)
p_g^κ / q_g^κ	Active/reactive power output of generator g
n_l ($\boldsymbol{n}_l$)	Integer number of new lines added to RoW l (vector form)
r_i^κ	Electricity load loss at bus i (MW)
s_i^κ	Wind power curtailment at bus i (MW)
x_l^D	Binary variable: 1 represents installing DTR in RoW l and 0 otherwise
$\boldsymbol{x}^\kappa, \boldsymbol{y}$	Vectors representing the 2nd- and 1st-stage decision variables, respectively
Q_l (R_l^κ)	Variable used to represent $n_l x_l^D$ ($x_l^D f_l^\kappa$)
V_i^κ	Voltage magnitude at bus i (V)
$V_{l,f}^\kappa (V_{l,t}^\kappa)$	Voltage magnitude of from- (to-) side node of RoW l
β	A continuous decision variable related to the Benders cut used in the master problem
$\theta_{l,f}^\kappa (\theta_{l,t}^\kappa)$	Phase angle of from- (to-) side node of RoW l (rad)

Parameters

a_l, b_l	Real and imaginary parts of y_{ij}, respectively (RoW l connects nodes i and j, $i \neq j$)
b_{l0}	Half of the shunt susceptance of a line in RoW l
c_l	Annualized cost of a new line in RoW l (\$/km)
c_l^{D1}, c_l^{D2}	Annualized cost of installing DTR at an existing line and at a new line in RoW l, respectively (\$/km)
$d_{i,\mathrm{p}}^\kappa$, $d_{i,\mathrm{q}}^\kappa$	Active and reactive load demand at bus i, respectively (MW, MVar)
$f_l^S / f_l^{D,\kappa}$	STR/DTR of a line in RoW l (MW)
$\bar{f}_l^\kappa$	Upper bound of $\lvert f_l^\kappa \rvert$ (MW)
$\bar{p}_g$	Maximum active power output of generator g (MW)
h	Number of hours in the study period (h)
$\bar{n}_l$	Maximum number of new lines allowed in RoW l
n_l^0	Initial number of lines in RoW l
p^κ	Probability of scenario κ
$q_g^{\min}$, $q_g^{\max}$	Minimum and maximum reactive power output of generator g, respectively
$M_{i,l}$, $\lvert M \rvert_{i,l}$	Element in row i and column l of the node-branch incidence matrix and its absolute value, respectively
$\underline{V}_i$, $\bar{V}_i$	Minimum and maximum voltage magnitude allowed at bus i, respectively
$\bar{W}_i^\kappa$	Maximum wind power generated at bus i (MW)
Z_{up}^ξ, (Z_{dn}^ξ)	Upper (lower) bound obtained after solving all slave problems (master problem) in iteration ξ
α	A conservative parameter used in (4), equal to one minus the prediction error of DTR
$\underline{\theta}$, $\bar{\theta}$	Minimum and maximum voltage phase angle allowed (set to 0 and 90°), respectively
$(\lambda_{1,i}^\kappa, \lambda_{3,i}^\kappa$ $\lambda_{4,l}^\kappa, \lambda_{2,l}^\kappa)$	Lagrangian multipliers associated with equality constraints (21d)-(21f), calculated using (22), respectively
$\varphi^{\kappa(,\xi)}$	Objective function of the κth slave problem (iteration ξ)
ρ_g	Generation costs of generator g (\$/MWh)

ρ_r, ρ_s Penalty costs for electricity load loss and wind spillage, respectively ($/MWh)

$\boldsymbol{A}_{(x_a)}$, $\boldsymbol{C}_{(x_c)}$ Coefficient matrices used in (16)-(19) and (21), $x_a = 1,2,3,4,\ x_c = 1,2,4,5$

$\boldsymbol{E}^{\kappa}_{(x_e)}$, $\boldsymbol{E}_5$ Parameter vectors used in (16)-(19) and (21), $x_e = 1,2,3,4$

I. Introduction

DTR calculates the maximum conductor capacity based on real-time ambient and conductor conditions. It provides a rapidly deployable and low-cost method of increasing line ratings, which can bring substantial economic benefits [1]. A dynamic thermal rating (DTR) system consists of sensing and communication devices and the software to determine the DTR for the conductors [2]. In recent years, relatively cheap, reliable, and accurate instruments for weather, sag, and conductor temperature monitoring have been developed [1]. Also, the costs of communication devices are decreasing. Therefore, DTR systems are now suitable for commercial installation [1, 3] and a number of demonstration projects have been set up. For example, partly funded by the U.S. Department of Energy's Smart Grid Demonstration Program, the New York Power Authority and Oncor Electric Delivery Company's projects have confirmed that, in most instances, up to 25% additional usable capacity can be achieved using DTR and that DTR systems can increase wind deliverability and relieve congestion [2], [4], [5]. An overview of a number of other projects can be found in [6].

The DTR is calculated via the heat balance equation [7]. In the heat balance equation, values for wind speed and direction, solar radiation, and ambient temperature are required to calculate the DTR. Many methods can be used to estimate the DTR of overhead transmission lines via the heat balance equation [8]. These methods are classified into monitoring systems based on weather, conductor temperature, tension, sag, and clearance. In [1], the strengths and weaknesses of various monitoring systems are evaluated. For example, sag and tension-based monitoring systems are likely to produce a more accurate line rating under contingency conditions, while weather-based monitoring systems are more suitable for normal system conditions. Therefore, selecting several different commercial off-the-shelf monitoring systems is recommended to obtain accurate DTRs in all system conditions [5], [8]. For example, tension, sag, and clearance-based monitoring systems are used in the Oncor project [4], which is one of the most successful DTR projects and therefore recommended to be repeated in other regions [8]. Another successful example is the New York Power Authority (NYPA)/EPRI project [5], where four different systems are installed, i.e., weather, conductor temperature, and sag-based monitoring systems, and the EPRI sensor systems.

Due to the benefits that DTR can bring, researchers have investigated how to integrate DTR into different power system operation and planning problems, including congestion management [9], unit commitment [10], wind power integration [11], distribution network operation [12], [13], time series modeling of the DTR [14], etc. Reference [15] summarized and compared four kinds of mathematical formulations for transmission expansion planning (TEP), i.e., a DC model, a transportation model, a hybrid model, and a disjunctive model. The DC model is relatively accurate but its power flow equation has non-linear terms [15], i.e., the product of an integer variable (representing investment decision) and a continuous variable (representing nodal phase angle). Solving the non-linear model is time-consuming. To address this issue, [16] proposed a Benders decomposition algorithm in which the slave problems are linearized such that the DC model can be solved very quickly. The DC model uses a DC power flow (DCPF) model that cannot consider voltage magnitude. However, voltage magnitude is important and needs to be maintained within a specified range. Recently, [17] proposed a decoupled linearized power flow (DLPF) model that can consider the voltage magnitude and phase angle and is more accurate than the DC power flow model.

To address future uncertainties in wind power and load demand, several new methods have recently been proposed for TEP, including stochastic programming [16], [18], robust optimization [19], chance-constrained method [20], probabilistic branch and bound method [21], etc. In stochastic programming, a large number of scenarios are used to accurately represent uncertainties. The original scenarios can be generated from historical data directly [22], Gaussian copula method [18], Monte Carlo simulation [23], or time-series modeling [24], etc. To avoid intractable computational burden, original scenarios need to be reduced to a relatively small number [23]. There are different types of scenario reduction methods including clustering methods such as K-means [25], backward and forward selection algorithms [26], improved forward selection algorithm (IFSA) [16], load- and wind-duration curve method [27], etc.

The DTR is significantly affected by the wind speed and can have a large range of variation. For example, the DTR can change by more than 1000 A in one hour as shown in [14]. In [28], the DTR is considered in the stochastic TEP model, which can obtain an investment plan for both new line constructions and DTR system installations at a minimum cost. However, in [28], DTR is essentially treated as a static thermal rating (STR) with a higher value and the DTR being smaller than the STR is simply treated as the DTR having no benefit and therefore not needing to be installed. This treatment cannot consider the significant influence of intermittent wind speed on the variation and uncertainty of DTR and creates an overload risk caused by the power flow on a line being smaller than the STR but larger than the DTR, which will accelerate the aging process and might even break the line and consequently cause a system blackout, e.g., the Northeast blackout of 2003 [29].

This paper focuses on integrating DTR into a TEP problem, because deferring/avoiding new investment is one of the most important benefits that can result from DTR [2]. Traditional TEP problems usually aim to create an investment plan for building new lines ensuring sufficient transmission capacity for the future load of power systems at a minimum cost. In addition to determining where to build new transmission lines, the TEP problem in this paper determines where to install DTR systems to fully realize their benefits. To address the problem mentioned in the previous paragraph, this paper proposes a new stochastic transmission expansion planning (STEP) model considering DTR that can avoid the overload risk; this is an important and innovative contribution. To the best of the authors' knowledge, this is the first time this risk has been considered when integrating DTR into power system planning problems.

Considering that the DLPF is more accurate than the DCPF, the DLPF is incorporated and extended into the DC model for the STEP in this paper and the solution method used in [16] is

extended to solve the STEP problem using the DC model with the DLPF. Stochastic programming is adopted to address the uncertainties associated with wind power, load demand, and DTR in STEP because it is a cost-effective way to deal with uncertainties. The uncertainty of the DTR is considered in the STEP model with the same logic as the uncertain wind power and load demand [16], [18], [22], [23], [28], i.e., use a large number of original scenarios to represent the uncertainty of the DTR and then reduce the original scenarios to a relatively small number of scenarios that are then used in the STEP problem. The IFSA is accurate and has a low computational burden and therefore is adopted for scenario reduction.

According to [30] and [31], the capability of transmission lines is usually governed by the thermal limit for lengths up to 80 km, by the line-voltage-drop limit in the 80 to 320 km range, and by the stability limit for lines longer than 320 km. Therefore, the extra capacity brought by the DTR being higher than the STR is only added to short lines up to 80 km in this paper. Managing the voltage magnitude is important for a line in the 80 to 320 km range because the line's capacity is limited by the line-voltage-drop but not the thermal rating. In other words, if the nodal voltage is not considered, applying DTR to a line in the 80 to 320 km range will cause a large voltage drop that is not allowed. This is the main reason for using DLPF instead of DCPF as the latter assumes unity voltage at each bus. STEP with consideration of stability issues, such as rotor angle stability [32], small signal stability, and transient stability, requires much further work [33] and is not considered in this paper; however, it does not affect the contribution of this paper because the DTR is used for short lines but the stability limit is for long lines.

Two ways of scenario reduction are performed in this paper. The first way directly uses the original scenarios as input to the IFSA. However, using this way cannot accurately represent the original scenarios even using a large number of reduced scenarios (RSs). The reason is that the scenarios associated with the DTR being lower than the STR have significant impacts on the STEP but they cannot be well represented by the RSs obtained in the first way. Therefore, a second way of scenario reduction is proposed: divide the original scenarios into two subsets according to whether or not the DTR is larger than the STR and then perform scenario reduction for each subset. The second way can better represent the original scenarios which will be shown in Section IV-D.

The contributions of the paper include 1) proposing a new STEP model that can consider not only the benefits but also the overload risk brought by the DTR, while existing literature considers neither the overload risk nor the uncertainty of DTR when integrating the DTR into TEP models, 2) proposing a new way of scenario reduction that can better represent the original scenarios when DTR is lower than STR compared to directly reducing all the original scenarios, and 3) incorporating an advanced DC power flow model, i.e., DLPF, into the new STEP model, which can provide more accurate results with less shedding costs (including both load and wind shedding) compared to the STEP using DCPF. The first two are the main contributions.

The remainder of the paper is organized as follows. The heat balance equation and the STEP model considering the DTR are detailed in Section II. Section III describes two ways of scenario reduction and a Benders decomposition method that is used to solve the STEP model. Simulation results are provided in Section IV. Finally, conclusions are drawn in Section V.

II. Stochastic Transmission Expansion Planning Considering Dynamic Thermal Rating

A. Heat Balance Equation for DTR

The heat balance equation can be represented by the balance of Joule heating $I^2R_{T_c}$, solar heating q_s, convective cooling q_c, and radiative cooling q_r:

$$I^2R_{T_c} + q_\mathrm{s} = q_\mathrm{c} + q_\mathrm{r} \quad (1)$$

where I is the conductor current and R_{T_c} is the electrical resistance of the conductor at conductor temperature T_c. The equations to calculate q_s, q_c, and q_r are available in [14] and are not repeated here to save space. Given the maximum allowable conductor temperature (set to 100 °C according to [14]) and the values of four affecting factors (wind speed and direction, solar radiation, and ambient temperature), the conductor current I can be calculated from (1) and is referred to as the DTR.

An example to calculate the DTR of a Drake 26/7 ACSR conductor is briefly given below. The parameters of the conductor and the heat balance model are available in Annex E.1 of [34]. Suppose the solar radiation is 1210 W/m^2, the ambient temperature is 40 °C, and the wind speed and direction are 0.61 m/s and 60°, respectively The electrical resistance $R_{T_c} = 9.3905 \times 10^{-5}$ Ω/m. Then, q_s is equal to 27.2 W/m, q_r is equal to 39.1 W/m, and q_c is equal to 77.6 W/m. Then, $I = \sqrt{(q_\mathrm{c} + q_\mathrm{r} - q_\mathrm{s})/R_{T_c}} = \sqrt{(39.1 + 77.6 - 27.2)/(9.3905 \times 10^{-5})} =$ 976 A according to (1), which is the DTR value. The detailed step-by-step calculation for this example is available in Annex E.1 of [34].

The DTR value used in the STEP model is evaluated from historical data using two sequential steps as illustrated in [35]: 1) estimate the four affecting factors in a right-of-way (RoW) using historical weather conditions from the RoW's nearby weather stations; and 2) evaluate the DTR value (called as the evaluated DTR value) in the RoW via (1) where the four affecting factors obtained in the previous step are used. This evaluated DTR value is used as the line's DTR value, i.e., $f_l^{D,\kappa}$ in the STEP model (2), and the DTR represents the line's real capacity.

B. STEP Model Considering DTR

The STEP model is given in (2). The objective function consists of the first-stage costs, which are independent of scenario κ (the first three terms in (2a)), and the second-stage costs, which are related to scenario κ (the last three terms in (2a)). The first-stage costs consist of the investment costs of building new lines and installing DTR systems for both existing and new lines. The second-stage costs consist of generation, wind power curtailment, and load shedding costs. Constraints (2b) and (2d) represent the active and reactive power balance at each bus, respectively. Constraint (2c) represents the active power flow on each line [17]. Constraints (2h) and (2i) represent the active power capacity limit of each line. Constraints (2e)-(2g) and (2j)-(2l) represent the lower and upper limits of the reactive power, voltage magnitude, and voltage phase angle, load shedding, generation, and wind power curtailment, respectively. Constraint (2m) represents the lower and upper limits of the number of new lines built in RoW l. Constraint (2n) indicates that x_l^D is a binary variable. Model (2) is a mixed-integer non-

linear programming model. Each constraint hereafter, where κ appears in the superscript, has $\forall \kappa \in \Omega_{rs}$.

$$\underset{n_l, x_l^D, p_g^\kappa, q_g^\kappa, s_i^\kappa, r_i^\kappa, V_i^\kappa, V_{l,f}^\kappa, V_{l,t}^\kappa, \theta_{l,f}^\kappa, \theta_{l,t}^\kappa}{\text{Minimize}}: \ \sum_{l\in\Omega} c_l n_l + \sum_{l\in\Omega}\left(c_l^{D1} n_l^0 + c_l^{D2} n_l\right) x_l^D + \sum_{\kappa\in\Omega_{rs}} p^\kappa h \left[\sum_{g\in\Omega_G} \rho_g p_g^\kappa + \sum_{i\in\Omega_B}\left(\rho_s s_i^\kappa + \rho_r r_i^\kappa\right)\right] \quad (2a)$$

$$\text{s.t.} \quad \sum_{l\in\Omega}\left(n_l^0 + n_l\right)\left(M_{i,l} f_l^\kappa\right) + \sum_{g|(i,g)\in\Lambda} p_g^\kappa + \overline{W}_i^\kappa - s_i^\kappa + r_i^\kappa - d_{i,\mathrm{p}}^\kappa = 0, \quad \forall i \in \Omega_B \quad (2b)$$

$$f_l^\kappa = a_l\left(V_{l,f}^\kappa - V_{l,t}^\kappa\right) - b_l\left(\theta_{l,f}^\kappa - \theta_{l,t}^\kappa\right), \quad \forall l \in \Omega \quad (2c)$$

$$\sum_{l\in\Omega}\left(n_l^0 + n_l\right)\left(|M|_{i,l} b_{l0} V_i^\kappa + M_{i,l}\left(-b_l\left(V_{l,f}^\kappa - V_{l,t}^\kappa\right) - a_l\left(\theta_{l,f}^\kappa - \theta_{l,t}^\kappa\right)\right)\right) + \sum_{g|(i,g)\in\Lambda} q_g^\kappa - d_{i,\mathrm{q}}^\kappa = 0, \quad \forall i \in \Omega_B \quad (2d)$$

$$q_g^{\min} \le q_g^\kappa \le q_g^{\max}, \quad \forall g \in \Omega_G \quad (2e)$$

$$\underline{V_i} \le V_i^\kappa \le \bar{V}_i, \quad \forall i \in \Omega_B \quad (2f)$$

$$\underline{\theta} \le \theta_{l,f}^\kappa, \theta_{l,t}^\kappa \le \bar{\theta}, \quad \forall l \in \Omega \quad (2g)$$

$$f_l^\kappa - \left(x_l^D f_l^{D,\kappa} + \left(1 - x_l^D\right) f_l^S\right) \le 0, \quad \forall l \in \Omega_1 \quad (2h)$$

$$-f_l^\kappa - \left(x_l^D f_l^{D,\kappa} + \left(1 - x_l^D\right) f_l^S\right) \le 0, \quad \forall l \in \Omega_1 \quad (2i)$$

$$0 \le r_i^\kappa \le d_{i,\mathrm{p}}^\kappa, \quad \forall i \in \Omega_B \quad (2j)$$

$$0 \le p_g^\kappa \le \bar{p}_g, \quad \forall g \in \Omega_G \quad (2k)$$

$$0 \le s_i^\kappa \le \overline{W}_i^\kappa, \quad \forall i \in \Omega_B \quad (2l)$$

$$0 \le n_l \le \bar{n}_l, \quad \forall l \in \Omega \quad (2m)$$

$$x_l^D \in \{0, 1\}, \quad \forall l \in \Omega, \quad (2n)$$

where $(\overline{W}_i^\kappa - s_i^\kappa)$ in (2b) represents the scheduled wind power generation at bus i. Although a linear power flow is used, model (2) is non-linear as both (2b) and (2d) have non-linear terms, i.e., the product of an integer variable, n_l, and other continuous variables such as $f_l^\kappa, V_{l,f}^\kappa, V_{l,t}^\kappa, \theta_{l,f}^\kappa$, and $\theta_{l,t}^\kappa$.

DTR and STR are related to the maximum current carrying capacity. For simplicity of expression, DTR and STR are used to refer to the maximum power carrying capacity in the rest of the paper. In (2h) and (2i), $x_l^D f_l^{D,\kappa} + \left(1 - x_l^D\right) f_l^S$ represents the capacity limit of a line in RoW l determined by the DTR if a DTR system is installed, i.e., $x_l^D = 1$. On the other hand, $x_l^D f_l^{D,\kappa} + \left(1 - x_l^D\right) f_l^S$ represents the capacity limit determined by the STR if a DTR system is not installed, i.e., $x_l^D = 0$. That is, $x_l^D f_l^{D,\kappa} + \left(1 - x_l^D\right) f_l^S$ represents the capacity limit whether a DTR system is installed or not. When n_l^0 or n_l is greater than 0, at least one line is in operation at RoW l and therefore $l \in \Omega_1$. Therefore, (2h) and (2i) are for both the existing lines and lines to be built. The thermal capacity (DTR or STR) of a candidate transmission line is assumed to be the same as an existing line at the same RoW.

Model (2) can realize the benefits of the DTR being larger than the STR by optimizing the value of x_l^D. However, it might suffer an overload risk caused by the power flow on a line being larger than the line's real capacity; this is explained and addressed in the next section.

C. Avoiding Overload Risk Due to STR Exceeding DTR

The current on a conductor can be divided into different zones, as shown in Fig. 1, according to its DTR/STR, long-term emergency rating (LTE), and short-term emergency rating (STE) values. The situation in each zone is summarized as follows:

- When the current is below the DTR (STR), i.e., Zone D (Zone R) in Fig. 1, it is always allowed.
- When the current is higher than the DTR (STR) but lower than the LTE, i.e., Zone L in Fig. 1, it can operate for a limited period of time (e.g., 24 hours per year [36]).
- When the current is higher than the LTE but lower than the STE, i.e., Zone S in Fig. 1, transmission operators are instructed to take immediate remedial steps, such as dropping load, to reduce the current on the conductor. If the high current in Zone S continues for more than 15 mins [36], the conductor should be tripped.
- Current exceeding the STE is not allowed and the conductor should be tripped immediately.

Zones S and L are both emergency rating zones and the current running in these zones will accelerate the aging of the conductor and should be avoided, i.e., the current should not exceed the STR/DTR.

As mentioned above, the DTR is usually larger than the STR, which can bring benefits as shown in the right-hand part of Fig. 1. In (2h) and (2i), $f_l^{D,\kappa}$ (f_l^S) represents the value of DTR (STR) as indicated in Fig. 1. However, sometimes the DTR is smaller than the STR as shown in the left-hand part of Fig. 1, which can result in overload risk if the DTR is not used. Specifically, if the power flow of a conductor is smaller than the STR but larger than the DTR, as shown in the 'Risk' part of Fig. 1, the power flow is running in an emergency-rating zone, which will accelerate the aging of the conductor. In particular, if the power flow is in Zone S, the conductor might be broken and even cause system blackout. Therefore, it is very important to prevent this overload risk. In the following, new constraints are designed and added to model (2) so that this risk is eliminated. Eqs. (2h) and (2i) are equivalent to

$$|f_l^\kappa| \le x_l^D f_l^{D,\kappa} + \left(1 - x_l^D\right) f_l^S, \quad \forall l \in \Omega_1 \quad (3)$$

The 'Risk' part of Fig. 1 can be represented by $f_l^{D,\kappa} < |f_l^\kappa| < f_l^S$. The idea of eliminating the risk is to add a hard constraint, i.e., (4), to prevent $f_l^{D,\kappa} < |f_l^\kappa| < f_l^S$ from occuring. In (4), only the relationship between $|f_l^\kappa|$ and $f_l^{D,\kappa}$ is considered because $|f_l^\kappa| < f_l^S$ is already guaranteed by (3).

$$\left(1 - x_l^D\right)\left(|f_l^\kappa| - \alpha f_l^{D,\kappa}\right) \le 0, \quad \forall l \in \Omega_1 \quad (4)$$

If DTR is installed ($x_l^D = 1$), (4) is relaxed and the power flow $|f_l^\kappa|$ is constrained by the evaluated DTR value $f_l^{D,\kappa}$ according to (3). If DTR is not installed ($x_l^D = 0$), (4) forces $|f_l^\kappa| \le \alpha f_l^{D,\kappa}$, where $\alpha < 1$ is a conservative parameter. The reason for using α is as follows. Note that the second stage of the STEP is modeling the operating-domain problems, e.g., day ahead or hour ahead operating problems. If a DTR system is installed on a line, i.e., x_l^D=1, the evaluated DTR described in Section II-A can be used as the $f_l^{D,\kappa}$ in the STEP model, i.e., using (3). On the other hand, if a DTR system is not installed on a line, i.e., x_l^D=0, the line's DTR value can only be predicted when it is used in the operating domain, e.g., predicting the four affecting factors that are then used in the heat balance equation to calculate the DTR value [37]. In this regard, it is not reasonable to limit the power flow at the exact value of $f_l^{D,\kappa}$ as the prediction of DTR has an associated error. Therefore, this paper proposes limiting the power flow to a conservative value that is lower than the evaluated DTR, i.e., $\alpha f_l^{D,\kappa}$, where α<1 as used in (4). Parameter α can be set to one minus the prediction error of DTR. For example, assume the prediction error is 10%, then α=1-0.1=0.9. Eqs. (3) and (4) together limit the power flow by the lower value of $\alpha f_l^{D,\kappa}$ and f_l^S if a DTR system is not installed.

The setting of α is affected by the accuracy of DTR prediction and the operator's conservativeness. In this paper, α is set to 0.9. A lower (higher) value of α will lead to a solution with higher (lower) cost because a lower (higher) rating is used, which will be further discussed in Sections IV-B and IV-C.

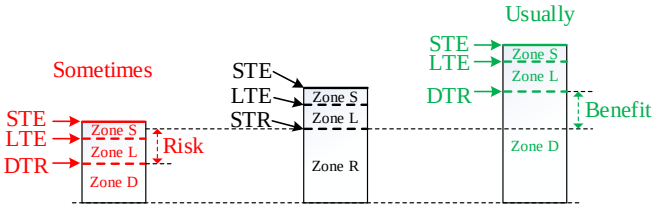

Fig. 1. The benefit of the DTR being larger than the STR and the risk resulting from the DTR being smaller than the STR.

D. Linearization of Constraint (4)

Constraint (4) has an absolute term and is non-linear, which complicates the resolution of the whole STEP model. To address this issue, (4) is linearized in this section. It can be reformulated as $(|f_l^\kappa| - \alpha f_l^{D,\kappa} - x_l^D|f_l^\kappa| + \alpha x_l^D f_l^{D,\kappa}) \le 0$, which is represented by (5) and (6) so as to remove the absolute term.

$$f_l^\kappa - \alpha f_l^{D,\kappa} - x_l^D f_l^\kappa + \alpha x_l^D f_l^{D,\kappa} \le 0, \quad \forall l \in \Omega_1 \tag{5}$$

$$-f_l^\kappa - \alpha f_l^{D,\kappa} + x_l^D f_l^\kappa + \alpha x_l^D f_l^{D,\kappa} \le 0, \quad \forall l \in \Omega_1 \tag{6}$$

Note that both x_l^D and f_l^κ are variables, i.e., both (5) and (6) have a non-linear term $x_l^D f_l^\kappa$. Considering that x_l^D is a binary variable and f_l^κ is a continuous variable, the non-linear term can be linearized by using another continuous variable, R_l^κ, to replace it, i.e., $R_l^\kappa = x_l^D f_l^\kappa$, subject to (7) and (8):

$$-\bar{f}_l^\kappa x_l^D \le R_l^\kappa \le \bar{f}_l^\kappa x_l^D, \quad \forall l \in \Omega_1 \tag{7}$$

$$f_l^\kappa - (1 - x_l^D)\bar{f}_l^\kappa \le R_l^\kappa \le f_l^\kappa + (1 - x_l^D)\bar{f}_l^\kappa, \quad \forall l \in \Omega_1 \tag{8}$$

where $\bar{f}_l^\kappa$ is the upper bound of $|f_l^\kappa|$ and $-\bar{f}_l^\kappa$ is the lower bound of $|f_l^\kappa|$. Then, the upper and lower bounds of R_l^κ are $\bar{f}_l^\kappa$ and $-\bar{f}_l^\kappa$, respectively. If $x_l^D = 0$, (7) is equivalent to $0 \le R_l^\kappa \le 0$ and (8) is equivalent to $f_l^\kappa - \bar{f}_l^\kappa \le R_l^\kappa \le f_l^\kappa + \bar{f}_l^\kappa$, i.e., (7) and (8) are equivalent to $R_l^\kappa = 0$. If $x_l^D = 1$, (7) is equivalent to $-\bar{f}_l^\kappa \le R_l^\kappa \le \bar{f}_l^\kappa$ and (8) is equivalent to $f_l^\kappa \le R_l^\kappa \le f_l^\kappa$, i.e., (7) and (8) are equivalent to $R_l^\kappa = f_l^\kappa$. That is, (7) and (8) can ensure that R_l^κ is equal to $x_l^D f_l^\kappa$. Therefore, (5) and (6) can be written as

$$(f_l^\kappa - \alpha f_l^{D,\kappa} - R_l^\kappa + \alpha x_l^D f_l^{D,\kappa}) \le 0, \ \forall l \in \Omega_1 \tag{9}$$

$$(-f_l^\kappa - \alpha f_l^{D,\kappa} + R_l^\kappa + \alpha x_l^D f_l^{D,\kappa}) \le 0, \ \forall l \in \Omega_1 \tag{10}$$

where R_l^κ needs to satisfy (7) and (8). By substituting (2c) into (9) and (10), one can obtain

$$a_l(V_{l,f}^\kappa - V_{l,t}^\kappa) - b_l(\theta_{l,f}^\kappa - \theta_{l,t}^\kappa) - \alpha f_l^{D,\kappa} - R_l^\kappa + \alpha x_l^D f_l^{D,\kappa} \le 0, \quad \forall l \in \Omega_1 \tag{11}$$

$$-a_l(V_{l,f}^\kappa - V_{l,t}^\kappa) + b_l(\theta_{l,f}^\kappa - \theta_{l,t}^\kappa) - \alpha f_l^{D,\kappa} + R_l^\kappa + \alpha x_l^D f_l^{D,\kappa} \le 0, \quad \forall l \in \Omega_1 \tag{12}$$

In summary, (4) is equivalent to (7), (8), (11), and (12). That is, linear constraints (7), (8), (11), and (12) are added to Model (2) to eliminate the overload risk caused by the power flow on a line being larger than the line's DTR.

E. Linearization of Objective Function (2a)

In the objection function, a non-linear term, i.e., $n_l x_l^D$, complicates the resolution of the whole STEP model. Therefore, it is linearized as follows to make Model (2) easier to solve. Note that $n_l x_l^D$ is the product of an integer variable and a binary variable. Let integer variable Q_l represent $n_l x_l^D$, i.e., $Q_l = n_l x_l^D$, and Q_l should satisfy (13) and (14):

$$0 \le Q_l \le \bar{n}_l x_l^D, \quad \forall l \in \Omega \tag{13}$$

$$n_l - \bar{n}_l(1 - x_l^D) \le Q_l \le n_l, \quad \forall l \in \Omega \tag{14}$$

If $x_l^D = 0$, (13) is equivalent to $0 \le Q_l \le 0$ and (14) is equivalent to $n_l - \bar{n}_l \le Q_l \le n_l$, i.e., (13) and (14) are equivalent to $Q_l = 0$. If $x_l^D = 1$, (13) is equivalent to $0 \le Q_l \le \bar{n}_l$ and (14) is equivalent to $n_l \le Q_l \le n_l$, i.e., (13) and (14) are equivalent to $Q_l = n_l$. That is, (13) and (14) can ensure that Q_l is equal to $n_l x_l^D$. Then, (2a) can be written as minimizing (15) subject to (13) and (14).

$$\sum_{l\in\Omega} c_l n_l + \sum_{l\in\Omega}(c_l^{D1} n_l^0 x_l^D + c_l^{D2} Q_l) + \sum_{\kappa\in\Omega_{rs}} hp^\kappa \left[\sum_{g\in\Omega_G} \rho_g p_g^\kappa + \sum_{i\in\Omega_B}(\rho_s s_i^\kappa + \rho_r r_i^\kappa)\right] \tag{15}$$

To write the models given later in explicit and self-contained forms, (2b)-(2l), (7), (8), and (11)-(14) are expressed in compact forms as follows. Eqs. (2b) and (2d) can respectively be written in compact forms as (16) and (17):

$$\boldsymbol{n}_l \boldsymbol{A}_{1,i} \boldsymbol{x}^\kappa + \boldsymbol{C}_{1,i} \boldsymbol{x}^\kappa = \boldsymbol{E}_{1,i}^\kappa, \quad \forall i \in \Omega_B \tag{16}$$

$$\boldsymbol{n}_l \boldsymbol{A}_{2,i} \boldsymbol{x}^\kappa + \boldsymbol{C}_{2,i} \boldsymbol{x}^\kappa = \boldsymbol{E}_{2,i}^\kappa, \quad \forall i \in \Omega_B \tag{17}$$

Eqs. (2h), (2i), (7), (8), (11), and (12) can be written as

$$\boldsymbol{A}_4 \boldsymbol{x}^\kappa + \boldsymbol{C}_4^\kappa x_l^D \le \boldsymbol{E}_4^\kappa \tag{18}$$

Eqs. (2c), (2e)-(2g) , and (2j)-(2l) can be written as $\boldsymbol{x}^\kappa \in \boldsymbol{X}^\kappa$ where $\boldsymbol{X}^\kappa = \{\boldsymbol{x}^\kappa \in R : \boldsymbol{A}_3 \boldsymbol{x}^\kappa \le \boldsymbol{E}_3^\kappa\}$. Eqs. (2m), (2n), (13), and (14) can be written as $\boldsymbol{y} \in \boldsymbol{Y}$ where $\boldsymbol{Y} = \{\boldsymbol{y} \in Z : \boldsymbol{C}_5 \boldsymbol{y} \le \boldsymbol{E}_5\}$. Let R and Z represent sets of real numbers and integer numbers, respectively. Now the complete STEP model with DTR can be given as (19):

$$\underset{\boldsymbol{x}^\kappa, \boldsymbol{n}_l, x_l^D, Q_l}{\text{Minimize}} \ \sum_{l\in\Omega} c_l n_l + \sum_{l\in\Omega}(c_l^{D1} n_l^0 x_l^D + c_l^{D2} Q_l) + \sum_{\kappa\in\Omega_{rs}} hp^\kappa \left[\sum_{g\in\Omega_G} \rho_g p_g^\kappa + \sum_{i\in\Omega_B}(\rho_s s_i^\kappa + \rho_r r_i^\kappa)\right] \tag{19a}$$

$$\text{s.t.} \quad \boldsymbol{n}_l \boldsymbol{A}_{1,i} \boldsymbol{x}^\kappa + \boldsymbol{C}_{1,i} \boldsymbol{x}^\kappa = \boldsymbol{E}_{1,i}^\kappa, \quad \forall i \in \Omega_B \tag{19b}$$

$$\boldsymbol{n}_l \boldsymbol{A}_{2,i} \boldsymbol{x}^\kappa + \boldsymbol{C}_{2,i} \boldsymbol{x}^\kappa = \boldsymbol{E}_{2,i}^\kappa, \quad \forall i \in \Omega_B \tag{19c}$$

$$\boldsymbol{A}_4 \boldsymbol{x}^\kappa + \boldsymbol{C}_4^\kappa x_l^D \le \boldsymbol{E}_4^\kappa \tag{19d}$$

$$\boldsymbol{x}^\kappa \in \boldsymbol{X}^\kappa; \quad \boldsymbol{n}_l, x_l^D, Q_l \in \boldsymbol{Y} \tag{19e}$$

III. Solution Method

A. Two Ways of Scenario Reduction

The first way of scenario reduction is to directly reduce the original scenarios using the IFSA, as introduced in the Introduction. The second way of scenario reduction divides the original scenarios into different subsets and reduces them separately; it consists of three steps as follows: divide the original scenarios into two subsets according to whether or not the DTR is larger than the STR; each subset of scenarios is used independently as data input for the IFSA to obtain RSs; and the RSs from both subsets obtained in the previous step are combined and used as scenario data input for the STEP.

The second way of scenario reduction is not specific for the STEP considering DTR and can be generalized for other stochastic programming problems that can be decomposed into a master problem and multiple sub-problems. For example, scenarios are used to represent the random outage of generators and transmission lines as well as load forecast errors in stochastic unit commitment problems in [38] and [39], where scenarios with multiple generators/transmission lines on outage probably have higher impacts (i.e., cause higher load shedding) on the

sub-problems than other scenarios and therefore deserve separate scenario reduction. The two general and key steps of the second way of scenario reduction are as follows. 1) In the original scenarios, identify an important subset of scenarios that probably have high impacts, e.g., have large objective values or violate constraints in the sub-problems. 2) Perform scenario reduction separately for the important subset. The reason for separately reducing the important subset is that relatively large number of RSs might be sampled from the important subset. If directly reducing all the original scenarios, a very large number of RSs might be required such that a sufficient number of RSs in the important subset can be sampled to accurately represent the original scenarios, which is not efficient.

B. Benders Decomposition

The complete STEP model is difficult to solve directly when there are a large number of scenarios. Benders decomposition is a suitable method to solve this STEP model. In the following, the Benders decomposition used to solve the complete STEP model is described. In the Benders decomposition method, an optimization problem is divided into a master problem and multiple slave problems. The master problem for STEP can be represented as

$$\underset{\boldsymbol{n}_l, x_l^D, Q_l, \beta}{\text{Minimize}} \quad \sum_{l\in\Omega} c_l n_l + \sum_{l\in\Omega}\left(c_l^{D1} n_l^0 x_l^D + c_l^{D2} Q_l\right) + \beta \tag{20a}$$

$$\text{s.t.} \quad \sum_{\kappa\in\Omega_{rs}} \varphi^{\kappa,\xi} + \sum_{\kappa\in\Omega_{rs}} \sum_{l\in\Omega} hp^{\kappa} \lambda_{2,l}^{\kappa,\xi} \left(n_l - n_l^{\xi}\right) + \sum_{\kappa\in\Omega_{rs}} \sum_{l\in\Omega} hp^{\kappa} \lambda_{4,l}^{\kappa,\xi} \left(x_l^D - x_l^{D,\xi}\right) \le \beta, \quad \forall \xi \tag{20b}$$

$$\boldsymbol{n}_l, x_l^D, Q_l \in \boldsymbol{Y}, \tag{20c}$$

where $\lambda_{2,l}^{\kappa,\xi}$ and $\lambda_{4,l}^{\kappa}$ are Lagrangian multipliers obtained after solving the slave problem as explained in the following. Variable β is equal to the sum of all sub-problems' objective when the Benders decomposition algorithm converges.

Considering (2b) is still a non-linear constraint, our previously proposed method [16] is used to formulate the slave problems as (21)-(22). The advantage of this formulation is that the slave problems are linear and have relatively small numbers of variables and constraints, which can significantly reduce the time required to solve the slave problems.

$$\underset{\boldsymbol{x}^{\kappa}, x_l^D}{\text{Minimize}} \quad \varphi^{\kappa} = hp^{\kappa}\left[\sum_{g\in\Omega_G} \rho_g p_g^{\kappa} + \sum_{i\in\Omega_B} (\rho_s s_i^{\kappa} + \rho_r r_i^{\kappa})\right] \tag{21a}$$

$$\text{s.t.} \quad \boldsymbol{x}^{\kappa} \in \boldsymbol{X}^{\kappa} \tag{21b}$$

$$\boldsymbol{A}_4 \boldsymbol{x}^{\kappa} + \boldsymbol{C}_4^{\kappa} x_l^D \le \boldsymbol{E}_4^{\kappa} \tag{21c}$$

$$\boldsymbol{n}_l^{\xi} \boldsymbol{A}_{1,i} \boldsymbol{x}^{\kappa} + \boldsymbol{C}_{1,i} \boldsymbol{x}^{\kappa} = \boldsymbol{E}_{1,i}^{\kappa} \,:\, \lambda_{1,i}^{\kappa}, \quad \forall i \in \Omega_B \tag{21d}$$

$$\boldsymbol{n}_l^{\xi} \boldsymbol{A}_{2,i} \boldsymbol{x}^{\kappa} + \boldsymbol{C}_{2,i} \boldsymbol{x}^{\kappa} = \boldsymbol{E}_{2,i}^{\kappa} \,:\, \lambda_{3,i}^{\kappa}, \quad \forall i \in \Omega_B \tag{21e}$$

$$x_l^D - x_l^{D,\xi} = 0 \,:\, \lambda_{4,l}^{\kappa}, \quad \forall l \in \Omega, \tag{21f}$$

where $p_g^{\kappa}, s_i^{\kappa}, r_i^{\kappa}$ in the objective function are elements of $\boldsymbol{x}^{\kappa}$ and n_l^{ξ} and $x_l^{D,\xi}$ are elements in the optimal solution of the master problem.

According to our previously proposed method [16], the $\lambda_{2,l}^{\kappa}$ used in (20b) can be calculated using

$$\lambda_{2,l}^{\kappa} = -\sum_{i=1}^{N} \lambda_{3,i}^{\kappa} \left(|M|_{i,l} b_{l0} V_i^{\kappa *} + M_{i,l}\left(-b_l\left(V_{l,f}^{\kappa *} - V_{l,t}^{\kappa *}\right) - a_l\left(\theta_{l,f}^{\kappa *} - \theta_{l,t}^{\kappa *}\right)\right)\right) - \sum_{i=1}^{N} \lambda_{1,i}^{\kappa} M_{i,l}\left(a_l\left(V_{l,f}^{\kappa *} - V_{l,t}^{\kappa *}\right) - b_l\left(\theta_{l,f}^{\kappa *} - \theta_{l,t}^{\kappa *}\right)\right), \ \forall l \in \Omega \tag{22}$$

where $V_i^{\kappa *}$, $V_{l,f}^{\kappa *}$, $V_{l,t}^{\kappa *}$, $\theta_{l,f}^{\kappa *}$, and $\theta_{l,t}^{\kappa *}$ are elements in the optimal solution of the corresponding slave problem (21).

In each iteration, the lower bound is calculated after solving the master problem using (23) and the upper bound is calculated after solving all of the κ slave problems using (24):

$$Z_{\text{dn}}^{\xi} = \sum_{l\in\Omega}\left(c_l n_l^{\xi} + \sum_{l\in\Omega}\left(c_l^{D1} n_l^0 x_l^{D,\xi} + c_l^{D2} Q_l^{\xi}\right)\right) + \beta^{\xi} \tag{23}$$

$$Z_{\text{up}}^{\xi} = \sum_{l\in\Omega}\left(c_l n_l^{\xi} + \sum_{l\in\Omega}\left(c_l^{D1} n_l^0 x_l^{D,\xi} + c_l^{D2} Q_l^{\xi}\right)\right) + \sum_{\kappa\in\Omega_{rs}} \varphi^{\kappa,\xi}. \tag{24}$$

The iterative process stops if the gap between the upper bound and the lower bound is smaller than a predetermined value, which is set to $0.001 \times \min(Z_{\text{up}}^{\xi}, Z_{\text{dn}}^{\xi})$. According to Chapters 5 and 6 of [40], the convergence of the Benders decomposition algorithm for a non-linear programming problem is guaranteed as long as the non-linear programming problem is convex when the complicating variables are fixed. The complicating variables are ones that, when temporarily fixed, render the remaining optimization problem considerably easier to solve. In this paper, the complicating variables are the integer/binary variables used to indicate how many lines to build and whether to install DTR systems, (i.e., n_l and x_l^D). When the complicating variables in model (19) are fixed, model (19) becomes linear and convex. Thus, the Benders decomposition can obtain the optimum of the non-linear model (19).

IV. Simulation

A. Test Systems and Data Sources

To verify the effectiveness of the proposed model and solution method, the STEP problem is solved on an IEEE reliability test system (RTS) system with 41 RoWs [20]. Using the same approach as [20], the original generation capacity and load are multiplied by three to cause congestion in the system. In addition, two wind farms are connected to buses 1 and 15. To show the scalability of the solution method, a modified IEEE 300-bus system [40] is also used. Buses with numbers higher than 9000 and the branches connected to them are deleted as they are distribution lines instead of transmission lines [41]. The original generation capacity and load are multiplied by 1.5 to cause congestion in the system. Two wind farms are connected to buses 1 and 49. The capacity of each wind farm is set to 850 MW. These loads and wind power capacities determined are considered as the base load and base wind capacity, respectively, in the modified test systems.

This paper uses the scale approach described in [16] to obtain multiple scenarios based on the base values of the load and wind capacity. Hourly load data from 2003 to 2005 for Ontario, Canada [16] are adopted. The number of original scenarios is 26304 (total hours in the 3-year period). Wind speed data from Environment Canada [14] for two cities (Windsor and Peterborough) in Ontario for the same period are converted into wind power using the same approach as [24]. Climate data (wind speed and direction, solar radiation, and ambient temperature) from Environment Canada for three cities (London, Toronto, and Wawa) in Ontario for the same period are used to calculate the DTR. The conductor used for DTR calculation is a 26/7 ACSR. Each cable is replaced by an overhead transmission line with the same capacity. For the original scenarios, each scenario represents one hour and its probability is equal to 1 divided by the total number of hours, i.e., 26304. For the RSs, the probability of each RS is determined by the scenario reduction method, i.e.,

IFSA. After performing scenario reduction, the probability of each RS is fixed.

As mentioned above, lines longer than 80 km need to be excluded from utilizing the extra capacity brought by the DTR being higher than the STR. This can be achieved by setting the scale factor to 1 if the DTR is larger than STR for lines longer than 80 km. RoWs 2, 21, 22, 23, and 30 in the IEEE RTS are longer than 80 km. The maximum number of new lines that can be added to each RoW for the two systems is set to 3 and 1, respectively. The total number of RSs is set to 7000, as further investigated in Sections IV-C and IV-E. The 'h' is equal to the total number of hours in a year (i.e., 8760). The penalty for load shedding is set to \$10000/MW. The values of several other parameters used are given in Table I. The STEP model is solved using MATLAB on a ThinkStation with 2 Intel Xeon E5-2650 V4 processors.

B. Investment Result

To show the effectiveness of the proposed STEP model, three versions of model (19) are solved using the Benders decomposition described in Section III on the modified IEEE RTS:

- case 1: α=0.9 (referred to as base case);
- case 2: α=1;
- case 3: Eqs. (7), (8), (11), and (12) are deleted from the model, i.e., the overload risk described in Sections II-C and II-D is not considered.

For convenience of expression, three terms, i.e., true total cost, estimated shedding cost, and true shedding cost are used in this paper, where the shedding includes both load and wind shedding. The *estimated* shedding cost is calculated via the last two terms in (19a) using the RSs (i.e., Ω_{rs} is used in the second row of (19a)) and the *true* total/shedding cost is calculated using all the original scenarios (i.e., the Ω_{rs} in the second row of (19a) is replaced by Ω_{os}).

The results of each case in terms of true total costs, number of new lines, and number of DTR installations are tabulated in Table II, and plans for new line construction are the same for cases 1 and 2, as tabulated in Table III. The plan for new line construction in case 3 is the same as case 1 except for the 11th RoW (there is only one new line construction for the 11th RoW in case 3). The plans for DTR installations in the three cases are not given in Table III as they are indicated when used in Fig. 2.

TABLE I
VALUES OF PARAMETERS USED IN THIS PAPER

c_l	c_l^{D1}	c_l^{D2}	ρ_g	ρ_s
\$1.5× 10^5/km	\$1500/km	\$750/km	\$10/MW	\$100/MW

TABLE II
SOLUTION OF CASES 1-3 IN TERMS OF TRUE TOTAL COST, NUMBER OF NEW LINES, AND NUMBER OF DTR INSTALLATIONS

Case	True total cost (M\$)	No. of new lines	No. of DTR installations
1	534.1	5	19
2	533.4	5	9
3	531.9	4	10

TABLE III
INVESTMENT PLAN FOR NEW LINE CONSTRUCTION IN CASES 1 AND 2

l	1	2	3	4	5	6	7	8	9	10	11	12	13	14	15	16	17
n_l	0	0	0	0	0	0	0	0	0	1	2	0	0	0	0	0	1
l	18	19	20	21	22	23	24	25	26	27	28	29	30	31	32	33	34
n_l	0	0	0	0	0	1	0	0	0	0	0	0	0	0	0	0	0

C. Effectiveness of the Proposed Model

In this sub-section, a case study is used to illustrate the effectiveness of the proposed model with respect to eliminating the overload risk caused by the power flow on a line being larger than the DTR as well as the power flow not being equal to the DTR value if a DTR system is not installed. For the results obtained in cases 1-3, the power flow of a line in each RoW in each of the 26304 original scenarios is compared with the line's DTR. No overload occurs in cases 1 and 2 in both test systems. However, overload occurs in case 3; the power flow is larger than the DTR by a multiple of 1149 and 21080 (sum of overloaded lines in all scenarios) in the 24-bus and 300-bus test systems, respectively.

The power flows in RoWs 24, 26, and 27 in scenario 22410 for cases 1-3 are shown in Fig. 2, where the circled numbers represent the index of the RoW. The main difference between Figs. 2a and 2c lies in the power flow in RoW 27. The DTR of each line in RoWs 24, 26, and 27 is 471.0694 MW. The power flows in RoW 27 in cases 1 and 3 are 430.3488 and 500.0 MW, respectively. The former is smaller than the DTR while the latter is larger. That is, there is overload in RoW 27 in case 3 as shown in Fig. 2c. As indicated in Figs. 2a and 2c, DTR systems are installed in RoW 27 in case 1 but not case 3. Because the DTR is installed in RoW 27 in case 1, the power flows are automatically adjusted such that the power flow in RoW 27 does not exceed the DTR value.

The main difference between cases 1 and 2 as shown in Figs. 2a and 2b lies in RoW 26. In case 2, the power flow in RoW 26 is equal to the DTR; however, a DTR system is not installed in this RoW so this situation is not reasonable because an accurate DTR value is not available without installing a DTR system. This is why a conservative value of the DTR, i.e., $\alpha f_l^{D,\kappa}$, is used in (4). Compared to case 2, the true total cost of case 1 is higher because the value of α is lower and, therefore, the power flow is restricted to a lower rating when a DTR system is not installed. On the other hand, setting α to a larger value is less conservative and results in a smaller value of true total cost.

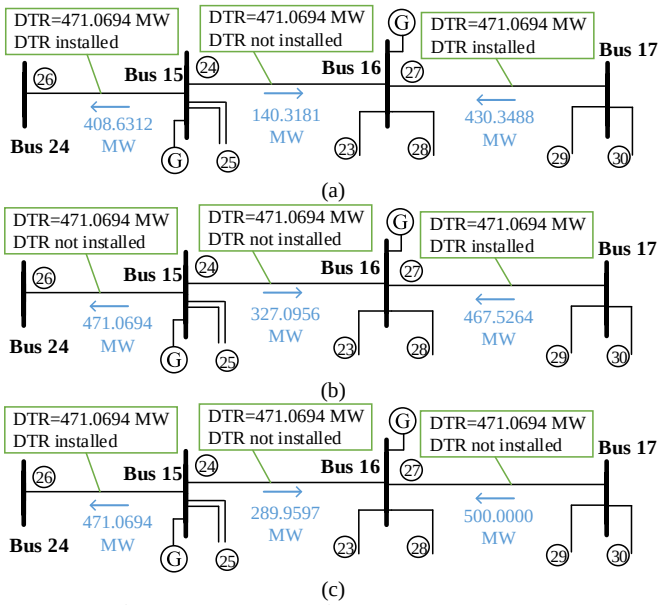

Fig. 2. Power flows in several RoWs for scenario 22410: a) case 1, b) case 2, and c) case 3.

In summary, the total cost for the solution in case 3 is slightly lower than in case 1 but there is overload; the total cost of the solution in case 2 is also slightly lower than in case 1 but the power flow can be limited exactly at the DTR of a line where no DTR system is installed, which is not reasonable. In case 1, the overload is eliminated and a conservative DTR value is used when no DTR system is installed. Note that this conclusion is also supported by simulation results using the modified IEEE 300-bus system, the details of which are not given here due to space limitations. Therefore, the proposed model should be used to not only realize the economic benefits due to the DTR being higher than the STR but also avoid the overload risk.

To verify the advantage of using the DLPF instead of the DCPF, the STEP using DCPF is also solved on the 24-bus system; the corresponding investment plan (solution) is called plan-DC (solution-DC). The true total cost of the STEP using DCPF is \$533.1M, which is lower than the base case (\$534.1M). The reason is that the voltage magnitude constraints are not considered in the DCPF, i.e., higher power flow is allowed in the DCPF than in the DLPF, and therefore the sub-problems will have smaller objective function values. Plan-DC is used to calculate the true total cost of the STEP using DLPF and the calculated value is \$543.8M, which is higher than the base case. Plan-DC actually has four new lines and 18 DTR installations, which is less than the base case investment plan (five new lines and 19 DTR installations). The true shedding cost of solution-DC calculated using the DLPF is \$18.3M, which is much higher than the base case (\$1.92M). In summary, the STEP using DCPF will lead to an insufficient investment plan that has higher true shedding cost than the solution of the STEP using DLPF. Therefore, it is necessary to use the DLPF instead of the DCPF. A more comprehensive comparison between the accuracy of the DLPF and DCPF is available in [17].

D. Number of Reduced Scenarios

In this sub-section, the suitable number of RSs is investigated. The STEP with DTR using different numbers of RSs (i.e., 4000, 5000, 7000, 10000, and 15000) is solved on both the 24-bus and 300-bus systems. Using the second way of scenario reduction, the 26304 original scenarios are divided into two subsets: the first subset (DTR≥STR) has 22944 elements and the second (DTR<STR) has 3360 elements. In the second way of scenario reduction, the number of RSs in the second subset is fixed at 3000, which will be discussed further in Section IV-F, and those in the first subset are 1000, 2000, 4000, 7000, and 12000.

The results associated with the second and first ways of scenario reduction are tabulated in Tables IV and V, respectively. In Tables IV and V, the 2nd column is the true total cost; the 3rd (4th) column is the estimated (true) shedding cost; the 5th column provides the relative error between the estimated and true shedding costs; and the 6th column is the solution time. Column 2 of Tables IV and V show that the true total cost is slightly lower when the number of RSs is larger. One reason is that the generation cost (equal to ~\$508 M) is a dominant portion of the true total cost and the total generation for different investment plans is almost the same considering the load shedding is small. Also, the investment cost is small compared to the generation cost and the difference of the investment costs will be compensated for by the difference of shedding costs. Therefore, the true total cost is not a good index to evaluate the quality of RSs. However, the shedding costs can be a good index as analyzed in the next paragraph.

Columns 4 and 5 of Tables IV and V show that both the true shedding cost and the relative error between the estimated and true shedding costs decrease as the number of RSs increases. The lower value given in column 5 indicates that the RSs can better represent the original scenarios. The lower value given in column 4 is associated with a better solution, because the load and wind shedding are less while the true total cost in column 2 remains almost constant. The last three rows of Table IV show that when the total number of RSs is equal to or higher than 7000, the true shedding costs in column 4 become relatively stable and the relative error in column 5 is relatively small. Therefore, the total RSs can be set to 7000 (i.e., the numbers of RSs in the 1st and 2nd subsets are 4000 and 3000, respectively) to balance accuracy vs. solution time.

The true shedding costs, relative error between estimated and true shedding costs, and solution time associated with both ways of scenario reduction for the STEP with DTR using different numbers of RSs in the 300-bus system are tabulated in Table VI. The 6th column in Tables IV and V and the 4th and 7th columns in Table VI indicate that the solution time increases as the number of RSs increases and the time consumed by the two ways of scenario reduction are not significantly different. This is because the solution time is mainly decided by how many iterations are needed to converge and how long an iteration takes. For Table VI, comparing its 5th-6th columns with its 2nd-3rd columns clearly shows that the second way is better than the first, as the former has lower values of true shedding cost and relative error.

TABLE IV
RESULTS OF STEP WITH DTR USING DIFFERENT RSS OBTAINED BY THE 2ND WAY OF SCENARIO REDUCTION IN THE 24-BUS SYSTEM (NUMBER OF RSS IN THE 2ND SET IS 3000).

Total No. of RSs	True total cost (M\$)	Est. shed. cost (M\$)	True shed. cost (M\$)	Rel. error (%)	Time (s)
4000	534.2	2.17	2.33	6.9	2986
5000	534.0	1.80	1.93	6.7	3528
7000	534.1	1.87	1.92	2.6	3708
10000	534.1	1.86	1.90	2.1	6532
15000	534.0	1.91	1.92	0.5	9158

TABLE V
RESULTS OF STEP WITH DTR USING DIFFERENT RSS OBTAINED BY THE 1ST WAY OF SCENARIO REDUCTION IN THE 24-BUS SYSTEM.

No. of RSs	True total cost (M\$)	Est. shed. cost (M\$)	True shed. cost (M\$)	Rel. error (%)	Time (s)
4000	538.5	1.51	13.84	89.1	3198
5000	539.2	1.64	14.54	88.7	3354
7000	534.3	2.58	4.71	45.2	3810
10000	534.6	3.72	4.48	17.0	6050
15000	534.4	3.83	4.48	14.5	8916

TABLE VI
RESULTS OF STEP WITH DTR USING DIFFERENT RSS OBTAINED BY BOTH WAYS OF SCENARIO REDUCTION IN THE 300-BUS SYSTEM.

Total No. of RSs	1st way of scenario red.			2nd way of scenario red.		
	True shed. cost (M\$)	Rel. error (%)	Time (s)	True shed. cost (M\$)	Rel. error (%)	Time (s)
4000	9.98	42.3	8564	2.49	16.5	11082
5000	2.46	41.4	9284	2.06	12.2	13584
7000	2.60	18.9	28566	2.09	10.3	25388
10000	2.24	12.1	39958	2.03	9.3	35338
15000	2.24	11.8	67546	2.02	7.7	61160

To ensure no overload occurs, a post-verification method can be used. That is, after obtaining an investment result, solve the sub-problem for each original scenario to check whether an overload occurs for the lines not installing DTR. If yes, a larger number of RSs is set and the STEP problem is re-solved, followed by the post-verification. We have post-verified all 20 solutions associated with those given in Tables IV-VI and found no overload. The numbers of RSs in the 1st and 2nd subsets have even been set to as low as 1000 and 100, respectively; again, the solution (4 new lines and 15 new DTR installations) obtained has no overload. That is, the solution provided by the proposed model usually does not involve overload risk. However, post-verification should be conducted to ensure no overloaded lines.

E. Impacts of Selecting Original Scenarios

To show the impacts of using different original scenarios on the investment solution, 5 different lengths of continuous time, i.e., 0.5, 1.0, 1.5, 2.0, and 2.5 years which are referred to as cases 4-8, respectively, are selected as the original scenarios. For cases 4-8, 10 different starting times are evenly set between the 1st hour and the 2.5th, 2.0th, 1.5th, 1.0th, and 0.5th years, respectively, of the three years of data used. The statistics (mean and standard deviation) of the shedding costs of the solutions obtained in the 10 different runs for each of cases 4-8 are tabulated in Table VII. As the purpose is to investigate the impacts of using different original scenarios, the impacts of scenario reduction are excluded by using all the original scenarios within the selected period of time, i.e., the Ω_{rs} in the second row in (19a) is replaced by Ω_{os}.

Row 3 of Table VII shows that the mean of shedding costs decreases as the length of time increases and approaches that of the base case. Row 4 of Table VII shows that the standard deviation of the shedding costs decreases. That is, when a longer period of time is used, the solution is more accurate. When the original scenarios in a relatively long period of time (e.g., 2.5 years) are used, the accuracy of the approach is slightly sensitive to the selection of the initial scenarios. However, as the length of time decreases below 2.5 years, the solution accuracy becomes more sensitive to the selection of the original scenarios.

TABLE VII
STATISTICS OF THE RESULTS OF STEP WITH DTR USING DIFFERENT LENGTHS OF ORIGINAL SCENARIOS IN THE 24-BUS SYSTEM.

Case		4	5	6	7	8	base
Length of time (year)		0.5	1.0	1.5	2.0	2.5	3.0
True shedding costs (M$)	Mean	21.0	6.50	3.48	2.36	2.02	1.92
	Standard deviation	5.9	5.8	1.7	1.6	0.1	--

F. Different Combinations of RSs from Two Subsets

For a total of 7000 RSs, different combinations of RSs from both subsets are used in the STEP using the 24-bus system and the results in terms of the estimated and true shedding costs and the relative error between them are shown in Table VIII (i.e., cases 9-14). The relative errors in cases 9-12 are quite large. In cases 13-14, although the relative errors are small, both the estimated and true shedding costs are high. That is, results of all cases 9-14 are worse than the base case given in the last row of Table VIII. If the number of RSs in one subset is fixed while that in the other subset decreases (increases), the solution accuracy decreases (does not increase) as shown in cases 15 and 16 (cases 17 and 18) of Table VIII. In summary, the accuracy decreases if the number of RSs decrease from 4000 for the 1st subset (3000 for the 2nd subset) while the accuracy does not increase by increasing the number of RSs beyond 4000 for the 1st subset (3000 for the 2nd subset). Therefore, 4000 and 3000 for the 1st and 2nd subsets is the best combination.

TABLE VIII
RESULTS OF STEP WITH DTR USING DIFFERENT COMBINATIONS OF NUMBERS OF RSS FROM EACH SUBSET IN THE 2ND WAY OF SCENARIO REDUCTION IN THE 24-BUS SYSTEM

Case	No. RSs. in the 1st Set	No. RSs in the 2nd Set	Est. shed. cost (M$)	True shed. cost (M$)	Rel. error (%)
9	5000	2000	2.29	4.54	49.6
10	5500	1500	2.38	9.24	74.2
11	6000	1000	2.27	8.82	74.3
12	4600	2400	2.64	4.99	47.1
13	4300	2700	4.51	4.54	0.7
14	3700	3300	4.58	4.62	0.9
15	3700	3000	4.66	4.70	0.9
16	4000	2700	4.50	4.54	0.9
17	4300	3000	1.88	1.92	2.1
18	4000	3300	1.87	1.92	2.6
base	4000	3000	1.87	1.92	2.6

G. Benefits Brought by DTR

To show the benefits attributed to the DTR, the STEP model with and without DTR is solved for different load levels. The load setting described in Section IV-A corresponds to a load level equal to 1. All of the loads are multiplied by 0.9 and 1.1 to obtain load levels of 0.9 and 1.1, respectively. The results in terms of costs, number of new lines built, and number of RoWs having DTR installation are tabulated in Table IX. Table IX shows that the differences between the total costs for STEP with and without DTR are $3.2M, $7.4M, and $7.7M for load levels of 0.9, 1, and 1.1, respectively, and that the difference between the numbers of new lines needed to be built for STEP with and without DTR are 2, 1, and 4 for load levels of 0.9, 1, and 1.1, respectively. From the 4th, 7th, and 8th lines of Table IX, the total costs for new line construction can be reduced by $3.8M, $3.3M, and $7.2M at costs of $708k, $1137k, and $1313k for installing DTR systems when the load levels are 0.9, 1, and 1.1, respectively. Therefore, we can conclude that using DTR can result in economic benefits by reducing the number of new lines that need to be built, and this benefit is more obvious when the load level is high.

TABLE IX
RESULTS OF STEP WITH AND WITHOUT DTR FOR DIFFERENT LOAD LEVELS

		Load level		
		0.9	1	1.1
Without DTR	Total cost ($M)	465.3	541.5	637.6
	Cost for new lines ($M)	13.4	26.1	53.7
	Number of new lines	6	6	12
With DTR	Total cost ($M)	462.1	534.1	629.9
	Cost for new lines ($M)	9.6	22.8	46.5
	Cost for DTR ($M)	0.708	1.137	1.313
	Number of new lines	4	5	8
	Number of DTR installations	13	19	23

V. CONCLUSION

In this paper, a new STEP model considering DTR was proposed. The model can determine the investment plan for both new line construction and DTR systems installation. The

model was linearized so it can be effectively solved by a Benders decomposition method. A modified IEEE RTS system and a modified IEEE 300-bus system were used to verify the effectiveness of the proposed model.

The simulation results show that if the power flow is larger than the DTR but smaller than the STR, using the STR will cause an overload in many lines. This overload can be avoided by using the proposed model; that is, the proposed model can not only realize the benefits that occur when the DTR is higher than the STR but also avoid the overload risk that occurs when the DTR is lower than the STR. The simulation results also show that 1) the second way of scenario reduction is superior to the first and 2) using the DTR can result in economic benefits by reducing the number of new lines that need to be built and this benefit increases as the load level increases. Moreover, the simulations have also investigated setting the number of RSs from each subset as well as the impacts of using different lengths of original scenarios.

REFERENCES

[1] D. Douglass, W. Chisholm, G. Davidson, I. Grant, K. Lindsey, M. Lancaster, D. Lawry, T. McCarthy, C. Nascimento, M. Pasha, J. Reding, T. Seppa, J. Toth, and P. Waltz, "Real-time overhead transmission-line monitoring for dynamic rating", *IEEE Trans. Power Del*., vol. 31, no. 3, pp. 921-927, 2016.

[2] U.S. Department of Energy, Dynamic Line Rating Systems for Transmission Lines–Smart Grid Demonstration Program, Topical Report, 2014.

[3] G. Migliavacca, Advanced technologies for future transmission grids. London: Springer-Verlag, 2013.

[4] Oncor Electric Delivery Company, Dynamic line rating--Oncor Electric Delivery Smart Grid Program, Final Report, 2013.

[5] A. Phillips, B. Clairmont, D. Childs, D. Reuger, D. Douglass, J. Bell, D. Birrell, Evaluation of Instrumentation and Dynamic Thermal Ratings for Overhead Lines, Final Report, 2013.

[6] S. Jupe, M. Bartlett, and K. Jackson, "Dynamic thermal ratings: The state of the art," in *CIGRE 21st International Conference on Electricity Distribution*, Frankfurt, France, 2011, pp. 1–4.

[7] CIGRE Working Group B2.43, *Guide for thermal rating calculations of overhead lines*, Technical Brochure 601, Paris, France, 2014.

[8] C.R. Black, and W.A. Chisholm, "Key considerations for the selection of dynamic thermal line rating systems", *IEEE Trans. Power Del.*, vol. 30, no. 5, pp. 2154-2162, 2015.

[9] F. Qiu and J. Wang, "Distributionally robust congestion management with dynamic line ratings," *IEEE Trans. Power Syst.*, vol. 30, no. 4, pp. 2198–2199, 2015.

[10] M. Nick, O. Alizadeh-Mousavi, R. Cherkaoui, and M. Paolone, "Security constrained unit commitment with dynamic thermal line rating", *IEEE Trans. Power Syst.*, vol. 31, no. 3, pp. 2014-2025, 2016.

[11] D.M. Greenwood, G.L. Ingram, and P.C. Taylor, "Applying wind simulations for planning and operation of real-time thermal ratings", *IEEE Trans. Smart Grid*, vol. 8, no. 2, pp. 537-547, 2017.

[12] M. Z. Degefa, M. Humayun, A. Safdarian, M. Koivisto, R. J. Millar, and M. Lehtonen, "Unlocking distribution network capacity through real-time thermal rating for high penetration of DGs," *Electr. Power Syst. Res.*, vol. 117, pp. 36 – 46, 2014.

[13] A. Safdarian, M.Z. Degefa, M. Fotuhi-Firuzabad, and M. Lehtonen, "Benefits of real-time monitoring to distribution systems: dynamic thermal rating", *IEEE Trans. Smart Grid*, vol. 6, no. 4, pp. 2023-2031, 2015.

[14] J. Zhan, C.Y. Chung, and E. Demeter, "Time series modeling for dynamic thermal rating of overhead lines", *IEEE Trans. Power Syst.*, vol. 32, no. 3, pp. 2172-2182, 2017.

[15] R. Romero, A. Monticelli, A. Garcia, and S. Haffner, "Test systems and mathematical models for transmission network expansion planning", *IEE Proceedings - Gener., Transm., Distrib*, vol. 149, no. 1, pp. 27-36, 2002.

[16] J. Zhan, C.Y. Chung, and A. Zare, "A fast solution method for stochastic transmission expansion planning", *IEEE Trans. Power Syst.*, vol. 32, no. 6, pp. 4684-4695, 2017.

[17] J. Yang, N. Zhang, C. Kang, and Q. Xia, "A state-independent linear power flow model with accurate estimation of voltage magnitude", *IEEE Trans. Power Syst.*, vol. 32, no. 5, pp. 3607-3617, 2017.

[18] H. Park, R. Baldick, and D.P. Morton, "A stochastic transmission planning model with dependent load and wind forecasts", *IEEE Trans. Power Syst*., vol. 30, no. 6, pp. 3003-3011, 2015.

[19] C. Ruiz and A. J. Conejo, "Robust transmission expansion planning", *European J. Opeartional Res.*, vol. 242, pp. 390-401, 2015.

[20] H. Yu, C.Y. Chung, K.P. Wong, and J.H. Zhang, "A chance constrained transmission network expansion planning method with consideration of load and wind farm uncertainties", *IEEE Trans. Power Syst.*, vol. 24, no. 3, pp. 1568-1576, 2009.

[21] J. Choi, T. Tran, A.A. El-Keib, R. Thomas, H. Oh, and R. Billinton, "A method for transmission system expansion planning considering probabilistic reliability criteria", *IEEE Trans. Power Syst.*, vol. 20, no. 3, pp. 1606-1615, 2005.

[22] H. Park, and R. Baldick, "Transmission planning under uncertainties of wind and load: sequential approximation approach", *IEEE Trans. Power Syst.*, vol. 28, no. 3, pp. 2395-2402, 2013.

[23] J. H. Roh, M. Shahidehpour, and L. Wu, "Market-based generation and transmission planning with uncertainties," *IEEE Trans. Power Syst.*, vol. 24, no. 3, pp. 1587–1598, Aug. 2009.

[24] R. Billinton, and W. Wangdee, "Reliability-based transmission reinforcement planning associated with large-scale wind farms", *IEEE Trans. Power Syst.*, vol. 22, no. 1, pp. 34-41, 2007.

[25] F. D. Munoz and J.P. Watson, "A scalable solution framework for stochastic transmission and generation planning problems", *Comput. Manag. Sci.*, vol. 12, pp. 491-518, 2015.

[26] H. Heitsch, and W. Romisch, "Scenario reduction algorithms in stochastic programming", *Comput. Optimization and Appl.*, vol. 24, no. 2-3, pp. 187-206, 2003.

[27] L. Baringo and A. J. Conejo, "Transmission and wind power investment," *IEEE Trans. Power Syst.*, vol. 27, no. 2, pp. 885–893, May 2012.

[28] M. Jabarnejad and J. Valenzuela, "Optimal investment plan for dynamic thermal rating using benders decomposition", *European J. Operational Res.*, vol. 248, no. 3, pp. 917-929, 2016.

[29] U.S.-Canada Power System Outage Task Force (2004). Final Report on the August 14, 2003 Blackout in the United States and Canada: Causes and Recommendations. [Online]. Available: https://www3.epa.gov.

[30] F. Kiessling, P. Nefzger, J. F. Nolasco, and U. Kaintzyk. *Overhead Power Lines: Planning, Design, Construction*. New York, USA: Springer, 2003.

[31] R. D. Dunlop, R. Gutman, P. P. Marchenko, "Analytical development of loadability characteristics for EHV and UHV transmission lines", *IEEE Trans. Power Apparatus Syst.*, vol. PAS-98, no. 2, pp. 606-617, 1979.

[32] S. Robak and K. Gryszpanowicz, "Rotor angle small signal stability assessment in transmission network expansion planning", *Elect. Power Syst. Res.*, vol. 128, pp.144-150, 2015.

[33] J. Quintero, H. Zhang, Y. Chakhchoukh, V. Vittal, and G.T. Heydt, "Next generation transmission expansion planning framework: models, tools, and educational opportunities", *IEEE Trans. Power Syst.*, vol. 29, no. 4, pp. 1911-1918, 2014.

[34] CIGRE Working Group B2.43, "Guide for thermal rating calculations of overhead lines," Technical Brochure 601, Paris, France, 2014.

[35] A. Michiorri, P. C. Taylor, and S. C. E. Jupe, "Overhead line real-time rating estimation algorithm: Description and validation," *Proc. IMechE Part A, J. Power Energy*, vol. 224, no. A3, pp. 293–304, 2010.

[36] CIGRE Working Group B2.36, "Guide for application of direct real-time monitoring systems," Technical Brochure 498, Paris, France, 2012.

[37] A. Michiorri and P. C. Taylor, "Forecasting real-time ratings for electricity distribution networks using weather forecast data," in *Proc. CIGRE 20th Int. Conf. Elect. Distrib.*, Prague, the Czech Republic, 2009.

[38] L. Wu, M. Shahidehpour, and T. Li, "cost of reliability analysis based on stochastic unit commitment", *IEEE Trans. Power Syst.*, vol. 23, no. 3, pp. 1364-1374, 2008.

[39] L. Wu, M. Shahidehpour, and Y. Fu, "Security-constrained generation and outage scheduling with uncertainties", *IEEE Trans. Power Syst.*, vol. 25, no. 3, pp. 1674-1685, 2010.

[40] A. J. Conejo, E. Castillo, R. Minguez, and R. Garcia-Bertrand, *Decomposition Techniques in Mathematical Programming*. New York, NY, USA: Springer, 2006.

[41] C.E. Murillo-Sánchez, R.D. Zimmerman, C.L. Anderson, and R.J. Thomas, "Secure planning and operations of systems with stochastic sources, energy storage, and active demand", *IEEE Trans. Smart Grid*, vol. 4, no. 4, pp. 2220-2229, 2013.

Junpeng Zhan (M'16) received B.Eng. and Ph.D. degrees in electrical engineering from Zhejiang University, Hangzhou, China.

He is currently a Postdoctoral Fellow in the Department of Electrical and Computer Engineering, University of Saskatchewan, Saskatoon, SK, Canada.

Weijia Liu received B.Eng. and Ph.D. degrees in electrical engineering from Zhejiang University, Hangzhou, China.

He is currently a Postdoctoral Fellow in the Department of Electrical and Computer Engineering, University of Saskatchewan, Saskatoon, SK, Canada.

C. Y. Chung (M'01-SM'07-F'16) received B.Eng. and Ph.D. degrees in electrical engineering from The Hong Kong Polytechnic University.

He is currently a Professor, the NSERC/SaskPower (Senior) Industrial Research Chair in Smart Grid Technologies, and the SaskPower Chair at the University of Saskatchewan, Saskatoon, SK, Canada.

Dr. Chung is an Editor of *IEEE Transactions on Power Systems*, *IEEE Transactions on Sustainable Energy*, and *IEEE Power Engineering Letters*. He is a Member-at-Large (Global Outreach) of the IEEE PES Governing Board.